JAMES | Journal of Advances in Modeling Earth Systems®

RESEARCH ARTICLE
10.1029/2025MS005135

The Influence of Open Boundary Conditions and Model Resolution on Shallow Cloud Organization in Atmospheric Large Eddy Simulations

Franciscus Liqui Lung[1,2], Christian Jakob[1,3], Fredrik Jansson[4], and Pier Siebesma[4,5]

[1]School of Earth Atmosphere & Environment, Monash University, Melbourne, VIC, Australia, [2]The ARC Centre of Excellence for Climate Extremes, Sydney, NSW, Australia, [3]The ARC Centre of Excellence for the Weather of the 21st Century, Sydney, NSW, Australia, [4]Department of Geoscience and Remote Sensing, Delft University of Technology, Delft, The Netherlands, [5]The Royal Netherlands Meteorological Institute, De Bilt, The Netherlands

Abstract An open boundary setup is presented in which a high-resolution (high-res) large eddy simulation (LES) is one-way nested in a low-resolution (low-res) LES. The high-res nested LES is compared to the periodic LES from Savazzi et al. (2023, https://doi.org/10.1175/jas-d-23-0098.1). Both simulations are forced by the regional weather model HARMONIE-AROME: the periodic LES via domain-averaged tendencies, and the open boundary setup via the boundaries of the low-res nested LES. The open boundary simulations inherit the full atmospheric state from the larger domains through frequent boundary updates, including developed cloud structures and their environmental states. Cloud structures are refined as they transition to higher-resolution simulations, with clouds breaking into smaller fragments while retaining their large-scale distribution. This results in larger, more organized clouds in the high-res nested LES compared to the periodic LES when cloud fractions are similar. The periodic LES has a stronger daily cycle in cloudiness, with days starting very cloudy and ending with clear skies, producing deeper and more intermittent clouds accompanied by more intense rainfall. This leads to greater variation in cloud structures, ranging from large clouds during cloudy periods to fewer, smaller clouds during low cloud cover. In contrast, the high-res nested LES maintains more constant cloud cover, with cloud top and size varying more gradually. The intermittent behavior of the periodic LES is explained by the applied horizontally averaged tendencies, which drive the domain toward stable or unstable conditions. Inheritance of the full atmospheric state allows the high-res nested LES to maintain larger, more organized clouds.

Plain Language Summary In this study, we compare two types of computer simulations that model clouds in detail. One simulation (high-res nested large eddy simulation [LES]) is part of a series of models, where each smaller model gets its cloud patterns and atmospheric state from a larger model that covers a bigger area but with less detail. The other simulation (periodic LES) uses atmospheric background conditions from a larger weather model, but does not receive any clouds. The results show that the periodic LES creates clouds that change quickly, shifting between cloudy periods with large clouds and times with only a few small, scattered clouds. On the other hand, the high-res nested LES has more gradual changes in cloud patterns. In the setup consisting of a series of models, clouds tend to break into smaller fragments as they transition from larger models with less detail to smaller ones with more detail. The inheritance of clouds in the high-res nested LES results in larger, more clustered clouds during periods of similar cloud cover, compared to the periodic LES.

Key Points:

- A setup, where a high-resolution large eddy simulation (LES) is nested in a lower-resolution LES forced by a regional model, is compared to a periodic LES
- Cloud structures are refined and broken into smaller fragments as they transition to a higher-resolution domain in the open boundary setup
- In the high-resolution nested LES, clouds are larger and more organized than those in the periodic LES during similar cloud fractions

Supporting Information:

Supporting Information may be found in the online version of this article.

Correspondence to:

F. Liqui Lung,
franciscus.liquilung@monash.edu

Citation:

Liqui Lung, F., Jakob, C., Jansson, F., & Siebesma, P. (2026). The Influence of open boundary conditions and model resolution on shallow cloud organization in atmospheric large eddy simulations. *Journal of Advances in Modeling Earth Systems*, *18*, e2025MS005135. https://doi.org/10.1029/2025MS005135

Received 24 APR 2025
Accepted 17 MAR 2026

Author Contributions:

Conceptualization: Franciscus Liqui Lung, Christian Jakob, Pier Siebesma
Formal analysis: Franciscus Liqui Lung
Methodology: Franciscus Liqui Lung
Software: Franciscus Liqui Lung, Fredrik Jansson
Supervision: Christian Jakob, Pier Siebesma
Visualization: Franciscus Liqui Lung
Writing – original draft: Franciscus Liqui Lung

1. Introduction

The formation and occurrence of different cloud patterns have caught our interest for a long time. Field and modeling campaigns have been dedicated to studying cloud organization (Blossey et al., 2013; Jansson et al., 2023; Siebesma et al., 2003; Stevens et al., 2021; van Zanten et al., 2011). One of the main drivers for studying cloud organization is the uncertainty it creates for global circulation models used for climate predictions. The 6th assessment report of the IPCC (Forster et al., 2021) states that the net cloud feedback is positive (0.42 W m^{-2} $°C^{-1}$), however with an uncertainty ranging from −0.10 to +0.94 W m^{-2} $°C^{-1}$, it is the largest contributor to the overall climate feedback uncertainty. Turbulence-resolving modeling studies have greatly increased our understanding of boundary layer cloud processes. However, the variability in the type of clouds in

Writing – review & editing: Franciscus Liqui Lung, Christian Jakob, Fredrik Jansson, Pier Siebesma

these studies is usually much less than what is found in field studies and satellite imagery (Schulz & Stevens, 2023). Especially on the mesoscale the variability in cloud fields is not fully understood.

Large eddy simulation (LES) is a tool well suited to study boundary-layer processes. With a resolution in the range of 10–100 m these simulations resolve most of the boundary-layer turbulence. Historically, LES was used mainly to study idealized cases (J. Deardorff, 1972; Lilly, 1966; Sommeria, 1976). More recently, with the increase in available computational power, LES is employed to study cloud organization and feedback mechanisms in more realistic test cases (e.g., Savazzi et al., 2023; Schulz & Stevens, 2023). Schulz and Stevens (2023) compare their large-domain LES results in the trades to satellite imagery and show that although average cloud coverage is captured well, LES struggles to capture the variability in cloudiness, especially stratiform clouds, which leads to an underrepresentation of mesoscale patterns with patches that are characterized by stratiform clouds. The difficulty in representing cloud fields stems from both the resolution limitations and the domain size limitations. Microphysical processes are parametrized in LES and so are the smallest turbulence scales. These create an uncertainty on the small scales that will influence rainfall and cloud formation (Sato et al., 2015; van Zanten et al., 2011). On the other hand the high resolution of LES limits possible domain sizes, which in turn limits the maximum cloud size (Janssens et al., 2025) and the accurate representation of mesoscale variation in atmospheric background conditions.

The research of Jansson et al. (2023) shows that given time, LES is capable of creating most mesoscale, shallow cumulus cloud patterns. They conduct multiple idealized LES in a range of different background settings and find both small-and large scale structures. To create observed cloud fields in a realistic setup, it is important to get the background and forcing conditions right. Heterogeneity in surface conditions and changing large scale conditions play an important role in the formation of cloud structures (Borgnino et al., 2025; Rieck et al., 2014; Simon et al., 2024). To allow for this, more and more LESs are implementing open boundary conditions (Heinze et al., 2017; Kadasch et al., 2021; Lac et al., 2018; Liqui Lung et al., 2024; Skamarock et al., 2021). In contrast to the traditional double periodic lateral boundary conditions, open boundary conditions allow an LES to be coupled to a coarser numerical weather model. This way spatially and temporally varying background conditions can be advected into the LES domain through the lateral boundaries. Open boundary conditions also allow for more complex surface conditions as it removes the periodicity constrain. Additionally, larger cloud structures will not feel the effect of their periodic copies when using open boundaries, which might allow for the formation of larger structures.

In this research we investigate the influence of using open boundary conditions in LES on the resulting cloud fields. We will compare the periodic LES from Savazzi et al. (2023) to a high-resolution (high-res) nested LES that is part of an open boundary setup. The high-res nested LES is one-way nested to a low-resolution (low-res) nested LES that is forced at its boundaries by a regional weather model. The periodic LES and high-res nested LES span the same time period and area in the scope of the EUREC^{4}A campaign (Stevens et al., 2021). The EUREC^{4}A campaign consists of a 5-week observational campaign near Barbados in the Caribbean during January/February 2020. Some of the goals of EUREC^{4}A are to study cloud feedback mechanisms, the influence of sea-surface heterogeneity on cloud formation and providing a new benchmark for future high-resolution simulations (Bony et al., 2017).

The goals of the paper are (a) to quantify the differences between the cloud fields of both simulations and (b) to investigate how the cloud structures change as they transition from a lower-resolution simulation to a higher-resolution simulation in the open boundary setup. Both the periodic LES and the open boundary setup aim to be as close to the observed case as possible by using the regional weather model HARMONIE-AROME (Bengtsson et al., 2017) to force them. The availability of two long-lasting large-domain simulations, one with periodic and one with open boundary conditions provides an unique opportunity to compare the cloud fields observed in both simulations and to discuss the influence of using an open boundary setup. The paper is structured as follows. First, we will describe the different models and simulation setups. Then we will describe the methodology used to analyze and compare the cloud fields of the different simulations. At last we will discuss the results and we will finish with conclusions.

Table 1
Main Differences Between the Periodic Large Eddy Simulation (LES), High-Res Nested LES and Low-Res Nested LES

	Periodic LES	High-res nested LES	Low-res nested LES
L_x, L_y, L_z (km)	150, 150, 8.3	520, 320, 8.3	1,440, 1,200, 8.3
Δx, Δz (m)	99.21, 20–120	156.25, 20–120	625, 20–120
z_{0m}, z_{0h} (mm)	0.010, 0.010	0.160, 0.032	0.160, 0.032
Microphysics	Two moment[a]	Two moment[b]	Two moment[b]
CDNC (cm^{-3})	50	70	70
SST	Daily hom. SST	Hourly het. SST	Hourly het. SST
SFS turbulence	Isotropic	Anisotropic	Anisotropic
Forcing	Tendency profiles	Boundary input	Boundary input

Note. From top to bottom: domain size, horizontal, and vertical gridsize, roughness lengths for momentum (z_{0m}) and heat (z_{0h}), microphysics scheme, cloud nuclei condensation number, sea surface temperature forcing, sub-filter scale turbulence scheme, large-scale forcing. [a]Khairoutdinov and Kogan (2000). [b]Seifert and Beheng (2001).

2. Simulation Setups

This section describes the different models and simulation setups used in this research. First, the setup of the regional weather model HARMONIE-AROME used to force both the periodic LES and the open boundary setup is described. Second, the LES setups are presented.

2.1. HARMONIE-AROME

Both the periodic LES and open boundary setup are forced by version c43 of HARMONIE-AROME (hereafter named HARMONIE). A description of version c40 is given by Bengtsson et al. (2017). Between versions c40 and c43, three parameterization schemes have been revised that together represent boundary layer processes: the cloud scheme, the turbulence scheme, and the shallow cumulus convection scheme. The main motivation for this revision is to improve the representation of low clouds. The differences between the physics of versions c40 and c43, together with a description of the parameterizations, are given by de Rooy et al. (2022). HARMONIE was used to simulate a domain of 3200 × 2025 km centered around Barbados with a horizontal gridspacing of 2.5 × 2.5 km. The simulation started on 1 February 2020 and is done in a climate setting, which means that the model is not reinitialized during the simulation and is running freely from the initial date. This configuration of HARMONIE is also known HCLIM (HARMONIE-Climate). To ensure that HARMONIE is running in a realistic environment, its boundary conditions are provided by ERA5.

2.2. Periodic Setup

The LES model used for the periodic LES and open boundary setup is the Dutch Atmospheric LES model (DALES) (Heus et al., 2010). DALES uses an anelastic approximation and employs a staggered Arakawa-C grid. The prognostic variables are the three velocity components (u, v, w), the liquid water potential temperature θ_l, the total water specific humidity (q_t), the rain water specific humidity (q_r), the rain droplet number concentration (N_r), the subfilter scale turbulence kinetic energy (e) and up to 100 active or passive scalars. The main differences between the periodic LES, high-res nested LES and low-res nested LES are summarized in Table 1.

The periodic LES has been conducted by Savazzi et al. (2023). The simulation period runs from 2 to 10 February. The simulation domain is 150 × 150 × 8.3 km with a grid spacing of about 100 m for the horizontal and a stretched vertical grid spacing between 20–120 m. A sponge layer is implemented for the top one-third levels. The simulation is initialized from horizontally homogeneous profiles derived from HARMONIE. The first 4 hours of the simulation (1 February 20:00–2 February 00:00 local time) are discarded, as during this spinup stage DALES is still developing turbulence. The surface boundary conditions are defined by a fixed daily prescribed homogeneous sea surface temperature (SST), taken from HARMONIE, and a fixed surface roughness of 0.01 mm. The surface fluxes for heat, momentum and moisture are obtained using Monin-Obukhov similarity theory. Large-scale dynamical forcing terms (tendencies) for momentum, temperature, and humidity are derived from HARMONIE. These large-scale forcings are homogeneous in the horizontal dimensions and include

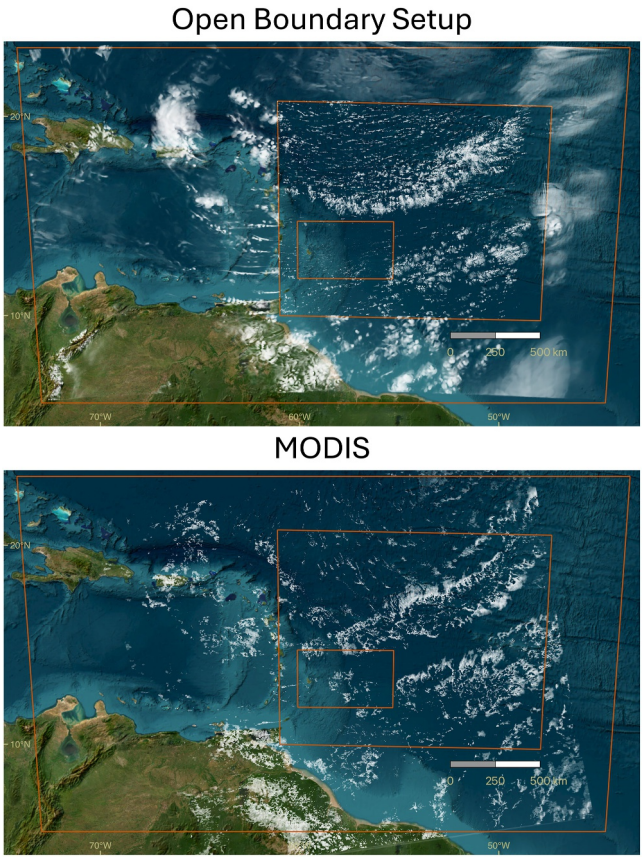

Figure 1. (Top panel) Simulated cloud albedo on 7 February at 13:15 local time, from the open boundary setup. The outer domain is the HARMONIE simulation, the middle domain the low-res nested large eddy simulation (LES) domain and the inner domain the high-res nested LES domain. The cloud albedo shown at a given location is taken from the highest-resolution simulation available. (bottom panel) Simulated cloud albedo derived from MODIS' cloud water path product (Platnick et al., 2017) for the same time. The simulation domains are added for spatial reference.

tendencies due to large-scale advection, pressure gradient, Coriolis force and a nudging term. The nudging term makes sure that the DALES profiles don't depart too much from the HARMONIE profiles. For more information on the derivation and application of these tendencies see Savazzi et al. (2023). A fifth-order central difference scheme is used for advection (Wicker & Skamarock, 2002) and the subfilter-fluxes are modeled using an eddy-diffusivity approach (J. W. Deardorff, 1980). Condensation is represented by a saturation adjustment scheme and for rain a two-moment scheme is used (Khairoutdinov & Kogan, 2000), with a constant cloud droplet number concentration (CDNC) of 50 cm^{-3}. Above the domain horizontally homogeneous profiles for pressure, temperature, humidity and ozone are used as input for a rapid radiation transfer model.

2.3. Open Boundary Setup

The DALES simulations for the open boundary setup have been conducted with the open boundary implementation described by Liqui Lung et al. (2024). The simulations span the period between 1 February and 12 February. Only the overlapping period with the periodic setup (2–10 February) is used for analysis. The setup consists of two one-way nested LES domains. The outer low-res nested LES, is forced by HARMONIE at its boundaries and steps down from HARMONIE's horizontal grid size of 2500 m to a grid size of 625 m. The inner high-res nested LES, is coupled to the low-res nested LES and has a horizontal resolution of 156.25 m. The setup is visualized in the top panel of Figure 1, which shows the simulation domains together with a simulated cloud albedo field. The locations of the low- and high-res nested LES domains are set to comply with the EUREC^{4}A model intercomparisson project, to which the simulations will be submitted. The bottom panel of Figure 1 shows cloud albedo for the same time obtained from the MODIS satellite (Platnick et al., 2017). This repeated nesting setup was chosen because, as shown by Liqui Lung et al. (2024), better results are expected when the grid size refinement factor does not exceed four. Furthermore, some turbulence and small-scale features can already develop in the low-res nested LES, providing the high-res nested LES with better boundary conditions compared to directly nesting it into HARMONIE.

The low-res nested LES domain spans a horizontal area of 1440 × 1200 km^2. In the vertical direction the grid layout is the same as the periodic LES. The simulation is initialized using 3D fields derived from HARMONIE and the lateral and top boundary conditions are supplied by hourly HARMONIE output. The surface boundary conditions are defined by hourly heterogeneous ERA5 sea surface temperatures and a fixed roughness length for momentum of 0.16 mm and for heat of 0.032 mm. The lateral, top and SST boundary conditions are linearly interpolated in time during the simulation. Synthetic turbulence is added to the lateral boundaries using the routine of Smirnov et al. (2001), which is implemented as described in Liqui Lung et al. (2024).

The high-res nested LES domain spans a horizontal area of 520 × 320 km^2. In the vertical direction the grid layout is the same as the periodic LES and low-res nested LES setups. The lateral and top boundary conditions are defined by 30 s output of the low-res nested LES. No synthetic turbulence is added at the boundaries because boundary input at high temporal frequency already contains turbulent structures. The surface, lateral and top boundary conditions are linearly interpolated in time during the simulation. The surface boundary conditions and initial state are defined similarly to the low-res nested LES. More details on the coupling of the two DALES simulations can be found in Appendix A.

Both the low- and high-res nested LESs use the same 5th order advection scheme as the periodic LES. They also use the same eddy-diffusivity approach for the subfilter-fluxes as the periodic LES, however the anisotropic adjustment described by de Roode et al. (2022) is applied. This allows for longer time-stepping, decreasing the computational costs of these large simulation setups. Horizontal homogeneous profiles, updated six-hourly, for

Table 2
Analysis Domains for Cloud Metrics

Simulations	$L_x \times L_y$ (km)	$\Delta x \times \Delta y$ (m)
Periodic and high-res nested LESs	150 × 150	≈150 × 150
High- and low-res nested LESs	520 × 320	625 × 625
Low-res nested LES and HARMONIE	1,440 × 1,200	2,500 × 2,500

temperature, pressure and humidity above the LES domain are used as input for the rapid radiation transfer model. The surface fluxes are calculated using Monin-Obukhov similarity theory. Just like the periodic LES, condensation is handled by a saturation adjustment scheme. For rain the two moment scheme of Seifert and Beheng (2001) is used with a constant CDNC of 70 cm^{-3}.

3. Methodology

To get an idea of the large scale background conditions of the periodic LES and high-res nested LES, daily mean, domain averaged profiles are constructed. The daily variation in cloudiness is then investigated using domain averaged cloud fraction profiles, followed by a domain variability study of CAPE and CIN.

Cloud organization is studied using the cloud metrics package of Denby and Janssens (2023), also described by Janssens et al. (2021). Janssens et al. (2021) look at cloud patterns in the trades, using 21 different cloud metrics. Employing principal component analysis, they show that the first four principal components can explain 82% of the variance and can thus describe most of the cloud patterns seen. In this research we will not calculate their four principal components, but to keep it more interpretable we will use two different metrics. Based on the advice given by Janssens et al. (2021), two metrics that they found were roughly orthogonal are used: mean open sky length and mean cloud length. The first one represents the mean length scale of a continuous open sky patch. The second one represents the mean length scale of all the clouds. To calculate the metrics, a cloud mask is required, which is obtained by defining a grid cell as cloudy when the simulation's liquid water path output is greater than 10 g/m^2. This non-zero threshold is selected to eliminate very thin cloud structures that may be the result of numerical artifacts.

The metrics are inherently sensitive to the resolution of the data used. With higher resolution data producing smaller length scales, as they can contain smaller clouds. Our main interest is on how the different simulations differ in larger-scale cloud structures. To mitigate the effect of the metric sensibility to the resolution of the data used and allow for a fair comparison between the simulations, metrics used to compare two simulations are obtained from analysis domains that span the same area and with the same resolution. Three different analysis domains are used, each to compare two simulations (see Table 2). In each comparison pair, we use the domain from the smaller, higher-resolution simulation and the resolution from the larger, lower-resolution simulation. This means that, before calculating the metrics for each analysis domain, a representative lower-resolution output is required from the higher-resolution simulation. This is obtained by coarse graining the liquid water path of the higher-resolution simulation. The coarse graining is achieved by averaging over a set number of grid cells. The lower-resolution simulation is clipped to the analysis domain. To compare the periodic LES with the high-res nested LES, the output of the periodic LES is first refined by a factor of two using nearest neighbor interpolation, which results in a gridspacing of 49.605 m. The refined output is then coarse grained by averaging over 3 × 3 gridcells, resulting in a gridspacing of 148.815 m. The high-res nested LES is clipped to the domain of the periodic LES. To compare the high-res nested LES to the low-res nested LES, the high-res nested LES is coarse grained by averaging over 4 × 4 grid cells and the low-res nested LES is clipped to the high-res nested LES domain. To compare the low-res nested LES to HARMONIE, the low-res nested LES is coarse grained by averaging over 4 × 4 grid cells and the HARMONIE output is clipped to the domain of the low-res nested LES. Whilst this method is imperfect in obtaining the true lower-resolution output of a higher-resolution simulation, we believe it is the fairest way of doing it. The metrics are used to study the distribution and time evolution of the cloud fields for the different simulations and to identify differences between the simulations.

4. Results and Discussion

The top panel of Figure 1 displays cloud albedo, derived from the simulated liquid water path using the method of Zhang et al. (2005), for the open boundary setup on 7 February at 13:15 local time. The cloud albedo at a given location is taken from the highest resolution simulation available. Animations for the full simulation period of the full setup and a close up of the high-res nested LES can be found in Movies S1 and S2. Examining the boundary between the low-res nested LES and HARMONIE, it is apparent that as clouds move from HARMONIE into the low-res nested LES domain, their structure becomes more refined. The higher resolution of the low-res nested

LES breaks down HARMONIE's cloud structures into smaller, more detailed formations at a finer scale. The same happens at the boundary between the high-res nested LES and the low-res nested LES, which can be better seen in Movies S1 and S2. The bottom panel of Figure 1 shows simulated cloud albedo, based on MODIS' Level 2 cloud water path product (Platnick et al., 2017), calculated using the same method of Zhang et al. (2005). MODIS' cloud water path product has a resolution of 1 km, which falls between the resolutions of HARMONIE and the low-res nested LES, being closer to the latter. Comparing the top and bottom panels of Figure 1, we can see that results of the low-res nested LES, in particular, show similar features to that of the MODIS image. The location, shape, and level of detail of the cloud structures are comparable. The locations of the clouds are, in part, inherited from HARMONIE. Based on this qualitative comparison, the refinement seen in the higher-resolution LESs is, for the time shown, consistent with MODIS. A quantitative analysis of the open boundary setup using satellite imagery is challenging, as DALES currently lacks a satellite simulator. Additionally, there is no satellite data available at the resolution of the high-res nested LES, making it difficult to validate the refinement occurring in this domain.

From Figure 1 and Movies S1 and S2, it can be seen that there are transition zones at the inflow boundaries, which are most prominent at the eastern boundaries of the high- and low-res nested LESs. In these areas, the models need to develop turbulence on their respective resolution scales, which can result in underdeveloped features. Judging from the cloud structures, the transition zone in the low-res nested LES can span up to approximately 250 km, whereas in the high-res nested LES it is much less prominent. Based on Liqui Lung et al. (2024), we expected the transition from the low-res to the high-res LES to be smooth, as the applied spatial refinement factor of 4 and the high temporal resolution of the boundary input data were shown to yield good results. A transition zone on the order of 1–5 km is to be expected, which is negligible relative to the total domain extent. The much larger transition zone observed in the low-res nested LES is due to two main factors: (a) the lower temporal resolution of the boundary input data (1 hr compared to 30 s), and (b) the differences in model physics between HARMONIE and DALES. We assessed the potential influence of these transition zones on our cloud metric results in Section 4.2 by repeating the analysis while progressively excluding larger areas near the boundaries. The results showed that, since the transition zones are small compared to the total domain size, their impact on the computed cloud metrics is negligible. Therefore, the results presented in this manuscript include the full analysis domain without excluding potential transition zones.

In the remainder of the results' section we will quantify the differences in cloud fields between the periodic LES and the simulations of the open boundary setup. First, we will compare the simulated background conditions and cloud cover of the high-res nested LES and periodic LES. Second, we will analyze the cloud structures created in each simulation using the mean cloud length and mean open sky length cloud metrics.

4.1. Atmospheric Background Conditions and Cloud Cover

Figure 2 shows the daily mean wind speed, wind direction, liquid water potential temperature, total specific humidity, the liquid water content, relative humidity and cloud fraction as a function of height averaged horizontally over the periodic LES and high-res nested LES domains. The black line indicates the mean over the entire analysis period.

The simulations have a comparable trend in wind speed with a wind speed that increases during the second half of the analysis period. In the boundary layer the periodic LES produces generally slightly higher wind speeds. The high-res nested LES has more shear near the surface, whereas the periodic LES shows more shear in the cloud layer. The wind direction is also very similar in both simulations, with Easterlies being the dominant direction. The high-res nested LES produces slightly more variation around the dominant wind direction.

The profiles of the liquid water potential temperature show some differences between the simulations. The periodic LES has more variability in its liquid water potential temperature in the subcloud layer with the mean being slightly warmer than the mean of the high-res nested LES. For the first 6 days (2–8 February) the high-res nested LES shows a strong increase in lapse rate at roughly 1.2 km, whereas the periodic LES shows the same feature at approximately 2.5 km. This corresponds to the lower cloud layer of the high-res nested LES, which can be seen in the liquid specific humidity, relative humidity and cloud fraction profiles. For the last 2 days (8–10 February) the shape of the profiles are more similar between the two simulations, with the periodic LES being slightly warmer. The total specific humidity profiles show that the high-res nested LES is slightly drier than the periodic LES and more well mixed in the subcloud layer with a steep gradient near the surface. The slightly drier and colder nature

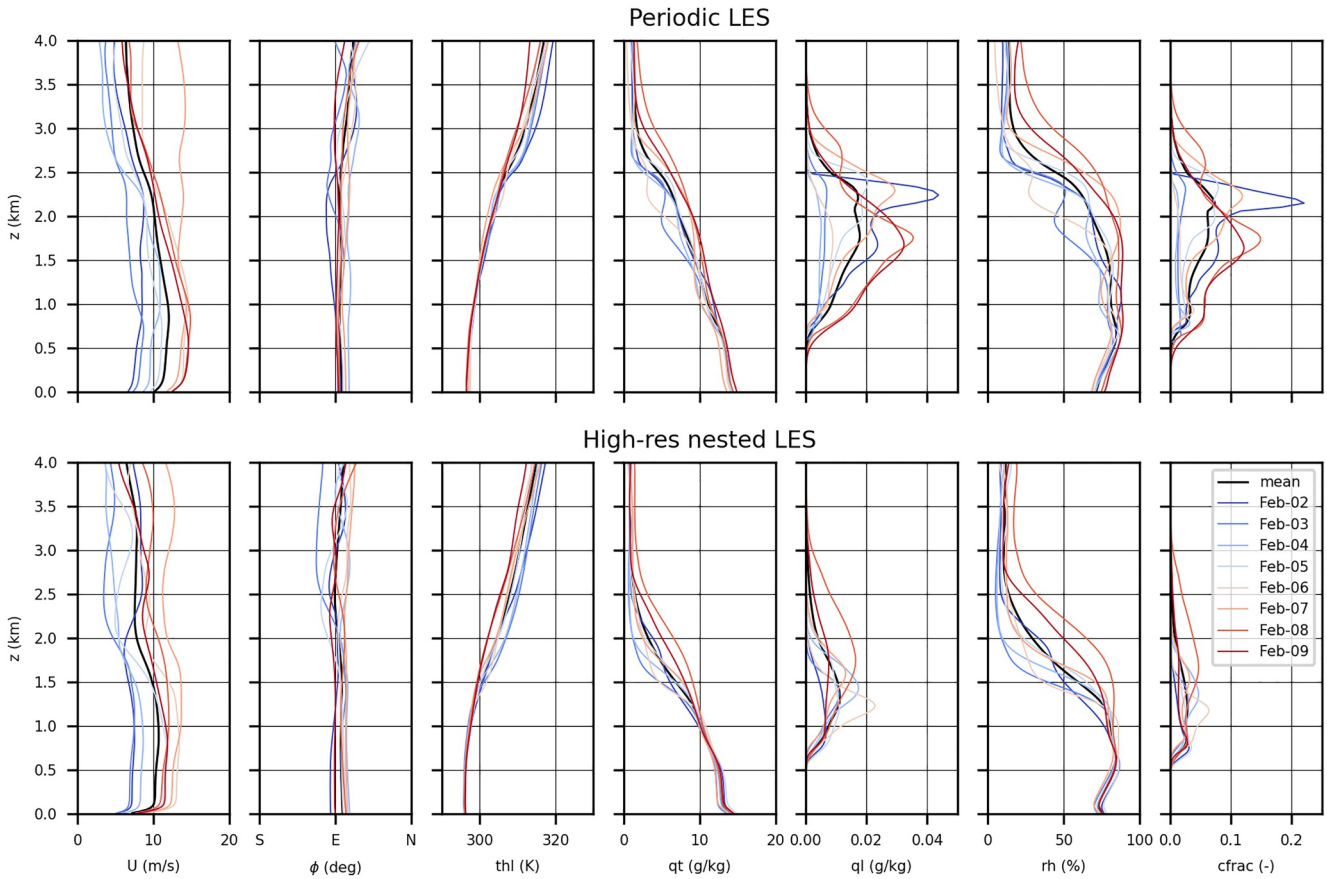

Figure 2. Daily domain averaged profiles for periodic large eddy simulation (LES) (top) and high-res nested LES (bottom) of the (left to right) wind speed, wind direction, liquid water potential temperature, total specific humidity, liquid specific humidity, relative humidity and cloud fraction. The black line denotes the average over the entire analysis period while the colored lines denote averages over individual days.

of the high-res nested LES results in similar relative humidity values in the subcloud layer compared to the periodic LES, except for a more humid near surface layer. The humidity and cloud fraction profiles also show that the cloud layer of the high-res nested LES is less deep compared to the periodic LES. The liquid specific humidity is lower for the high-res nested LES on 2, 5, 7–9 February and similar or higher for the other days. This is a direct result of the lower/higher cloud fractions that can be seen in the cloud fraction profiles. It should be noted that the high liquid water content of the periodic LES for the 2 February could still be a spinup artifact. The shape of the profiles is also different across the simulations, with the high-res nested LES profiles being more bottom to mid heavy and the periodic LES being more mid to top heavy. We can conclude that the large-scale background conditions for the two simulations are similar in terms of wind speed/direction total specific humidity and temperature, which was to be expected as they are both forced by HARMONIE albeit in different ways. From the liquid water related variables and cloud fraction profiles we can however already see that the resulting clouds differ between the two simulations.

When comparing these profiles to the nested simulation results of Schulz and Stevens (2023), it can be seen that their findings are more consistent with those of the high-res nested LES. Both their simulated and Barbados cloud radar-derived cloud fraction profiles show predominantly bottom-heavy structures for most days, with cloud fractions peaking near cloud base (approximately 800 m) at values between 0.05 and 0.1, followed by a gradual decay over a roughly 2 km-deep cloud layer.

To get an idea of the daily variation in cloudiness, Figure 3 shows the domain mean cloud fraction as a function of height for the periodic LES and high-res nested LES (right panels), as well as the temporal standard deviation normalized by the mean of the domain mean cloud fraction (left panel). In the right panels the orange line indicates the domain average surface precipitation rate and the black line the domain cloud top height which was,

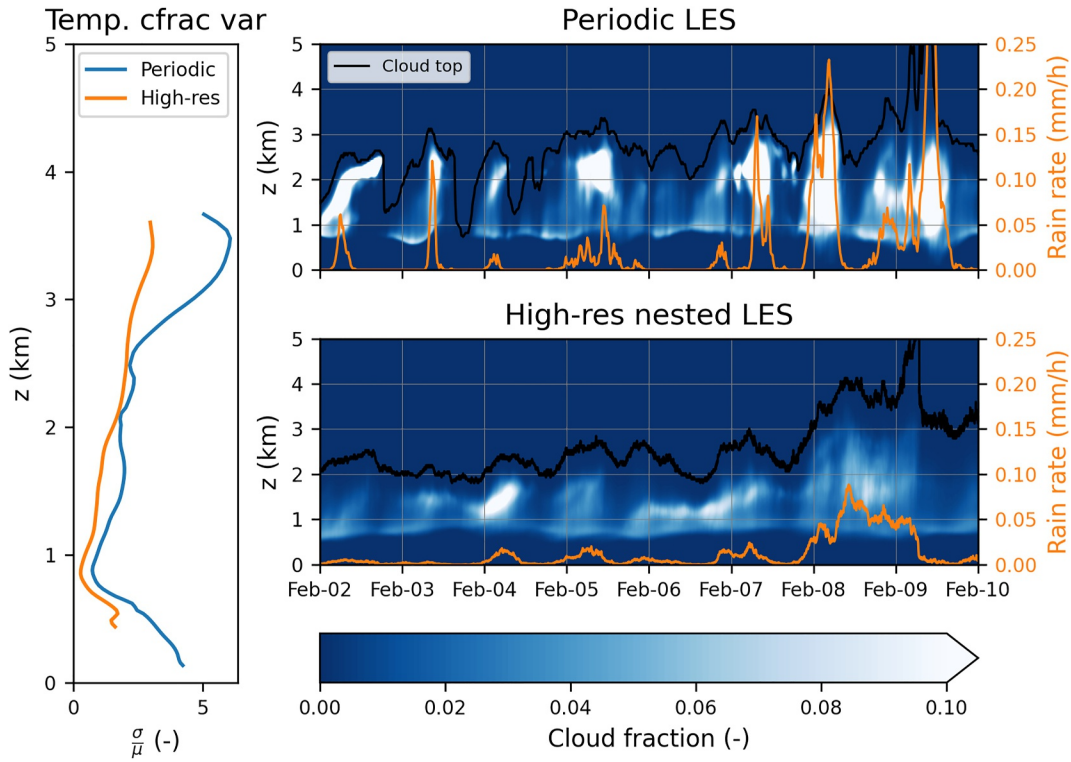

Figure 3. (Left panel) Temporal variation, standard deviation normalized by mean, of cloud fraction as a function of height for the periodic large eddy simulation (LES) (blue) and high-res nested LES (orange). (right panels) Time evolution of the domain average cloud fraction profile (colored), the domain average surface precipitation (orange) and the domain cloud top height (black line) for the periodic LES (top) and high-res nested LES (bottom). The gray gridlines for the time axis denote midnight local time.

similar to Savazzi et al. (2023), defined as the height where the domain average liquid specific humidity drops below 0.0001 g kg^{-1}, above the height where q_l maximizes.

Both simulations show a daily cycle, with cloudiness peaking around sunrise, followed by precipitation that partly dissipates the clouds, leading to a reduction in cloud cover by sunset. The magnitude of the daily cycle is however much larger for the periodic LES than for the high-res nested LES, with days starting completely cloudy and ending with clear skies. Clouds are more intermittent, penetrate deeper and rainfall is more intense in the periodic LES. The high-res nested LES on the other hand has a much more constant cloud cover. The rapid growth of clouds in the periodic LES is also accompanied by an increase in cloud base height, whereas cloud base height in the high-res nested LES varies much more gradually. The intermittent deep clouds and the variation in cloud base height result in a larger normalized temporal cloud fraction variation for the periodic LES in the left panel of Figure 3. The simulations exhibit consistent day-to-day variation in terms of precipitation and cloud depth, except for 3, 8, 9 February. On the 3 February the periodic LES creates a deep cloud layer with a peak in precipitation whereas the high-res nested LES does not. On 8 February and 9 February, the timing of precipitation differs between the two simulations. The periodic LES shows two distinct peaks in precipitation, while the high-res nested LES exhibits more consistent, lower levels of precipitation.

The daily cycle in cloudiness that was seen in Figure 3 agrees with the results of Vial et al. (2023), who studied the daily cycle in cloudiness using 10 year winter radar data at Barbados. Their composite daily cycle also shows that the overall cloudiness is lowest during daytime, while clouds deepen during nighttime with a maximum cloud cover before sunrise. They found that daily cloud cover variation is mainly due to variation in deep clouds (1.3−4 km) whereas very shallow clouds (<1.3 km) exhibit a very weak daily cycle. In agreement with the results of Vial et al. (2023), both the periodic and high-res nested LESs have the largest cloud fraction variation for deep clouds. However, partly due to the variation in cloud base height, the periodic LES also shows a large variation in cloud fraction for shallow clouds.

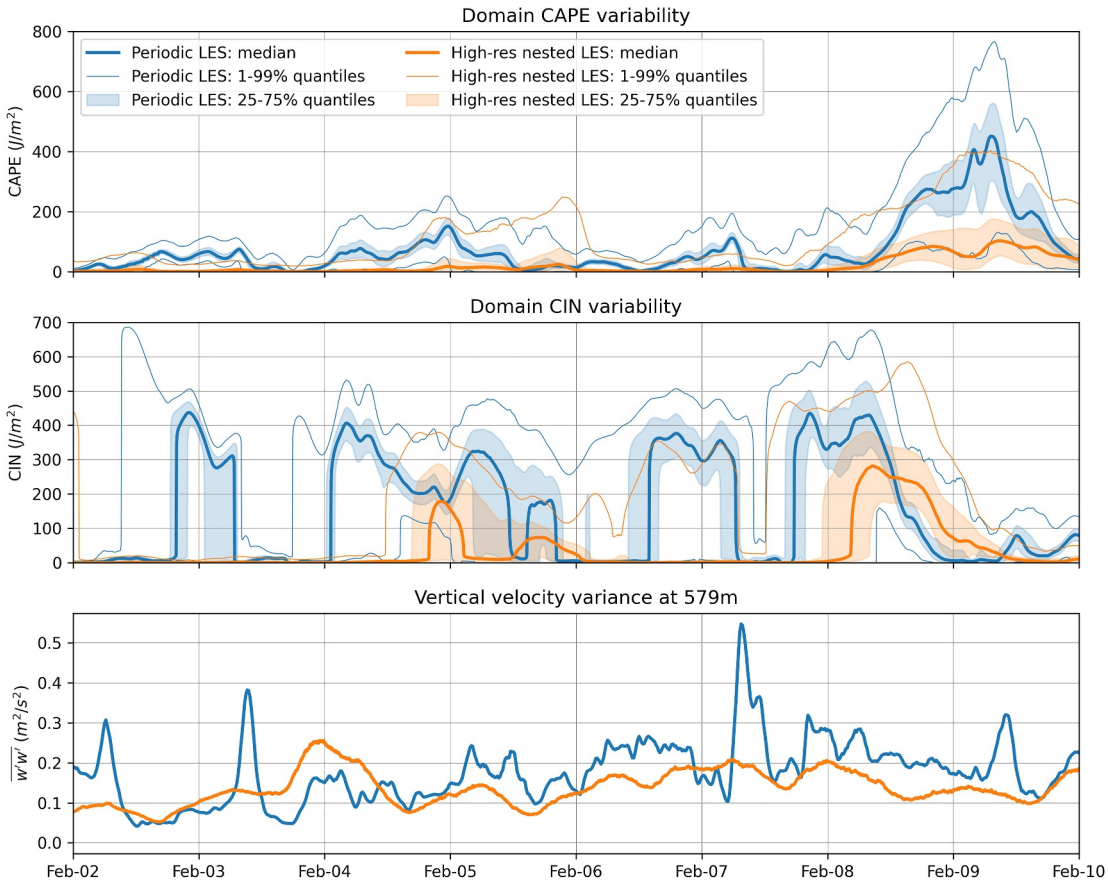

Figure 4. Time evolution of the domain CAPE (top), CIN (middle), and vertical velocity variance at 579 m for the periodic large eddy simulation (LES) (Blue) and high-res nested LES (orange). The shaded areas show the 25–75% quantiles, the thick line the median and the thin lines the 1–99% quantiles. The gray gridlines for the time axis denote midnight local time.

To investigate the causes of the different behaviors in cloud cover between the periodic LES and the high-res nested LES, Figure 4 shows the domain variability of CAPE (top), CIN (middle), and the 579 m domain vertical velocity variance (bottom). These are used to assess how the cloud cover transitions relate to atmospheric instability within the domains. For CAPE and CIN, the figure presents the median, 1–99% quantiles, and 25–75% quantiles for the periodic LES (blue) and the high-res nested LES (orange). For the periodic LES, peaks in cloud cover on 3, 5, 7, and 9 February coincide with increases in CAPE across the majority of the domain, as indicated by the significant increases in the 25–75% quantile range. In contrast, the high-res nested LES shows such a significant increase in CAPE across the majority of its domain only on 8 and 9 February, with magnitudes that remain considerably lower than those in the periodic LES. Most of the variation in CAPE for the high-res nested LES occurs in the 99% quantile. The closer spacing between the 1–99% and 25–75% quantiles in the periodic LES suggests that a larger portion of its domain transitions between stable and unstable conditions over time, whereas in the high-res nested LES these transitions are more localized.

A similar behavior is seen in the domain CIN time series. The periodic LES shows more frequent and pronounced transitions between high and low CIN values, with generally larger magnitudes compared to the high-res nested LES. This indicates stronger temporal fluctuations in boundary-layer stability, consistent with the more intermittent cloud cover behavior of the periodic simulation seen in Figure 3. In contrast, the high-res nested LES maintains lower CIN values overall and shows fewer domain-wide transitions, suggesting that its stability evolves more gradually over time and more locally.

The dynamical response to these instability variations can be seen in the vertical velocity variance timeseries. The periodic LES shows more variation in the produced vertical velocity variance, with large peaks corresponding to the peaks in cloudiness on 2, 3, 7, and 9 February. These sudden spikes in vertical velocity variance align with the

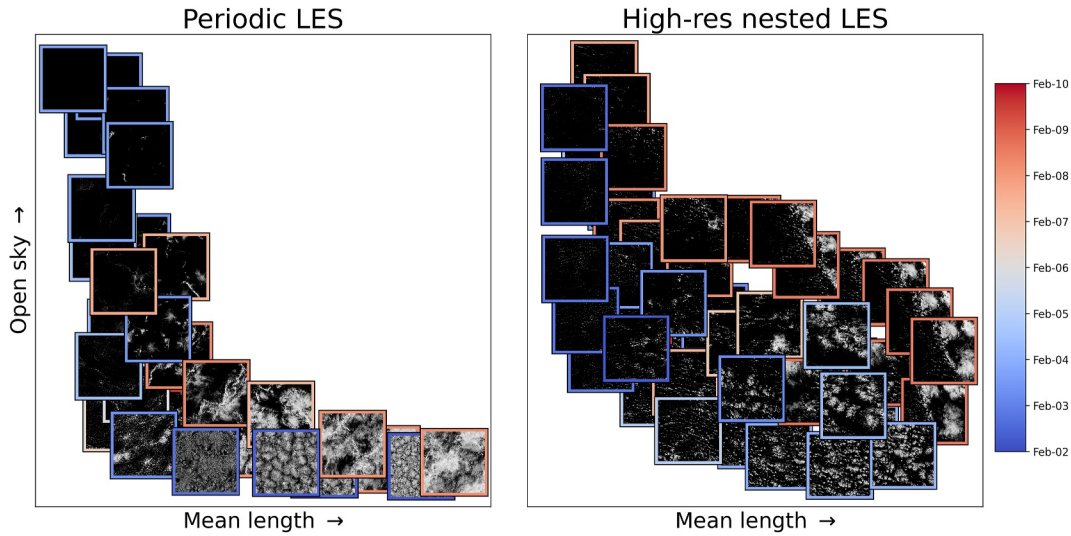

Figure 5. Selection of cloud images plotted against their mean open sky and mean cloud length parameters for the periodic large eddy simulation (LES) (left) and high-res nested LES (right). The colored frame around each image indicates the time. The axes are scaled differently for both panels to highlight variability.

intermittend cloud cover behavior found in Figure 3. In general the increased vertical velocity variances align with the domain stability CAPE and CIN metrics. The vertical velocity variance for the high-res nested LES varies more smoothly, showing increased values that correspond to the increased cloudiness on 4, 5, 7, and 8 February.

Overall, these results indicate that transitions between stable and unstable regimes occur more homogeneously and domain-wide in the periodic LES, compared to the more localized behavior of the high-res nested LES. This difference likely arises from the way large-scale forcing is applied. The periodic LES is driven homogeneously by horizontally averaged tendencies, which drive the entire domain toward either stable or unstable conditions. In contrast, the high-res nested LES is driven through its lateral boundary conditions, which provide a full atmospheric state from larger-scale models and allow for greater spatial variability and a more realistic evolution of local instability.

4.2. Cloud Organization

Cloud organization in the periodic LES and open boundary setup is analyzed using the mean open sky and mean cloud length metrics. To obtain a feeling of how the space spanned by these two metrics looks like, a selection of simulated cloud fields plotted against their cloud metrics is shown in Figure 5, similar to Figure 3 from Janssens et al. (2021). The results are shown for the periodic LES and high-res nested LES, obtained for the periodic LES analysis domain. To highlight the variability of the generated cloud fields, the axes are scaled differently for each simulation. Therefore, the location of images should not be compared between the two panels. In the bottom right of each window, the images are found with the largest cloud structures for each simulation, with little clear sky in between. In contrast, the top left of each window shows the images with very small cloud lengths and large clear sky areas, with the extreme being completely cloud-free. The bottom left contains images with small scattered clouds that have small patches of clear sky in between. The mean open sky length also provides insight into the clustering of clouds. For similar cloud fractions, a homogeneous scattered cloud field will have a shorter open sky length than one where clouds are clustered within certain areas of the domain. Both simulations produce a variety of different cloud structures. However, the almost completely cloudy scenes produced by the periodic LES are not produced by the high-res nested LES.

To quantify the differences between the cloud fields of both simulations, the distribution of all cloud images in the cloud metric space is shown in Figure 6. The first row shows the results of the periodic LES and high-res nested LES for the periodic LES analysis domain. The second row shows the results of the high- and low-res nested LESs for the high-res nested LES analysis domain. The third row shows the results of the low-res nested LES and HARMONIE simulations for the low-res nested LES analysis domain. The histograms are clipped at the

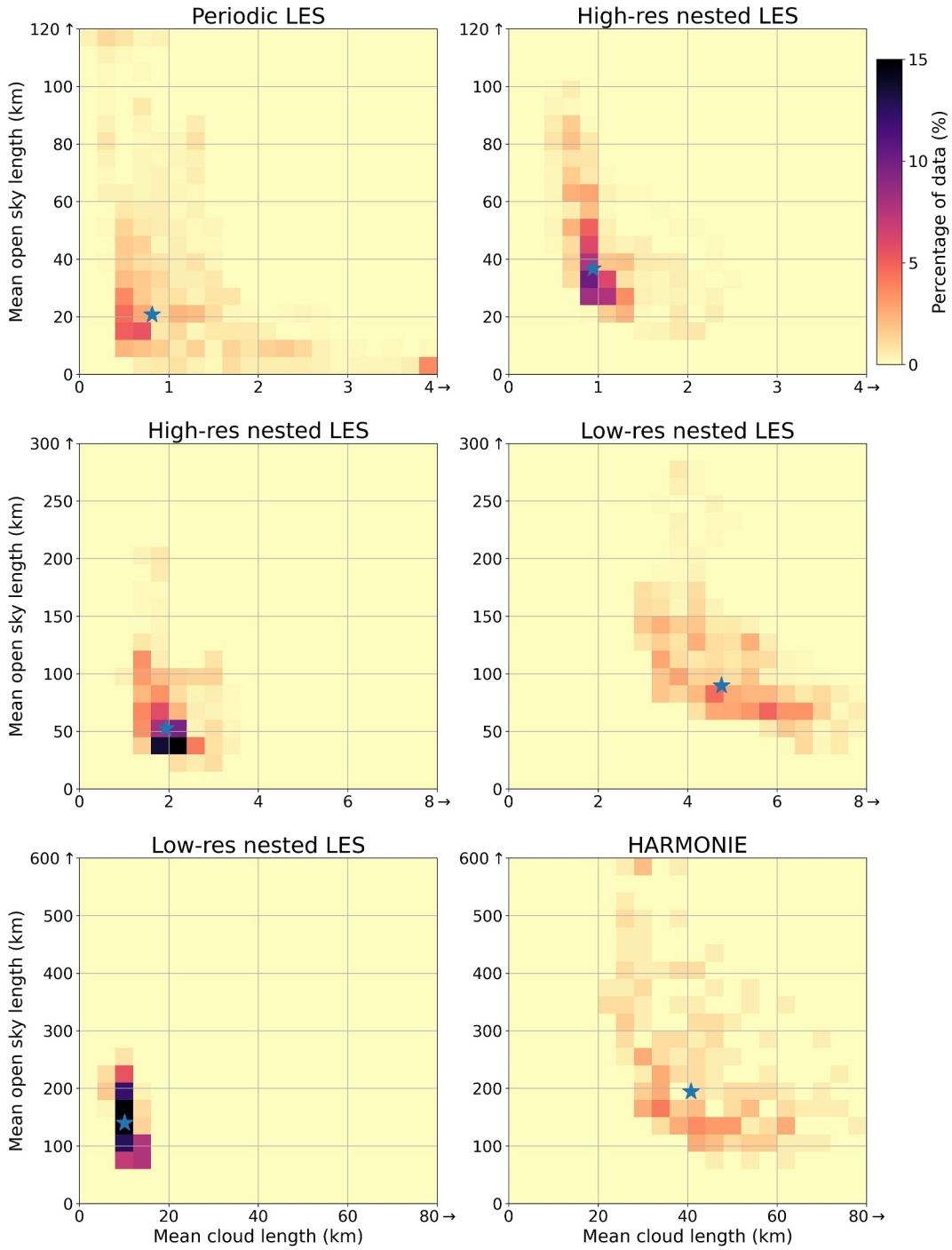

Figure 6. Distribution of cloud images in the cloud metric spaces. Each row represents a different analysis domain used to compare the simulations in the corresponding columns. The histograms are clipped at the maximum displayed values, and samples with metrics greater than these are assigned to the largest bin. The median of the cloud images is shown by the blue star.

maximum displayed values, and samples with metrics greater than these are assigned to the largest bin. The median of all cloud images is denoted by the blue star.

The first row of Figure 6 highlights the larger spread of cloud scenes produced by the periodic LES compared to the high-res nested LES. While the high-res nested LES does not produce fully cloud-free or completely cloudy

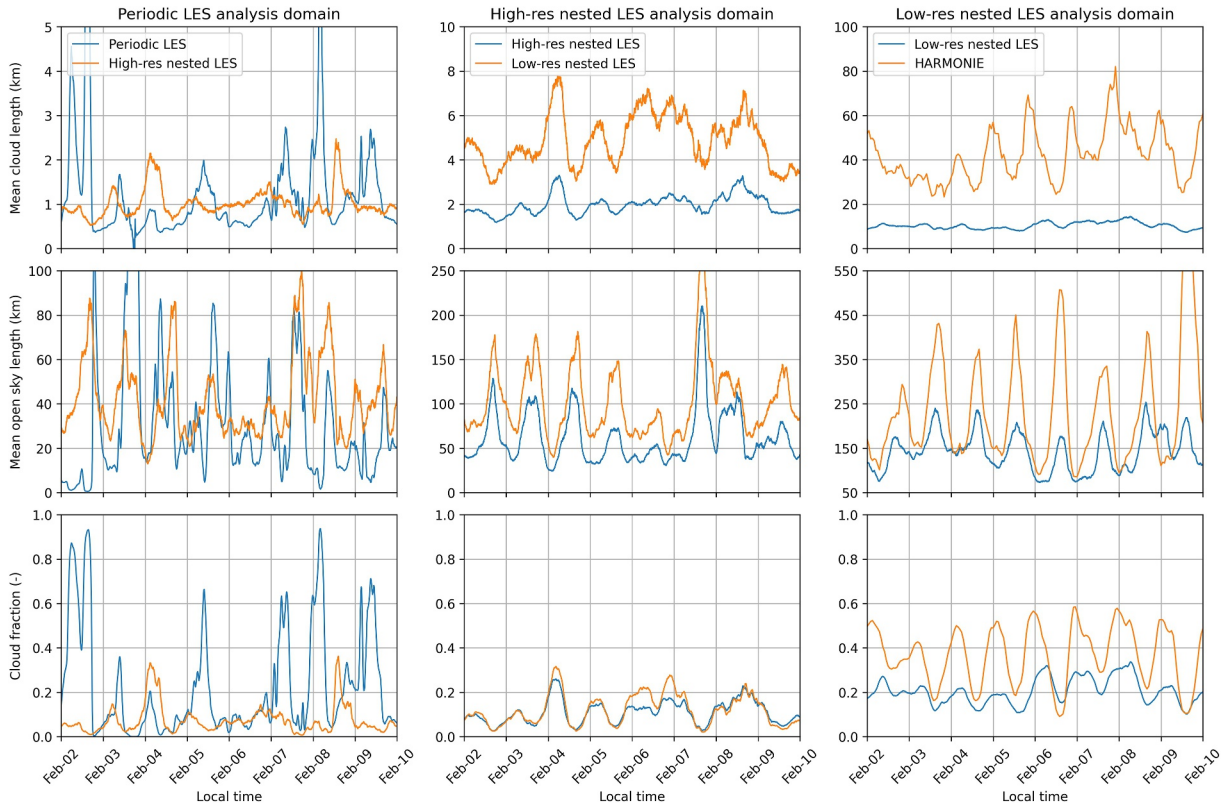

Figure 7. Timeseries of the cloud metrics. Each column represents a different analysis domain, similar to the rows of Figure 6. The rows show the mean cloud length, mean open sky length, and cloud fraction metrics. For each analysis domain, the higher-resolution simulation is shown in blue and the lower-resolution simulation in orange.

images, the periodic LES does, which can be attributed to the stronger daily cycle observed in Figure 3. The median mean cloud and open sky lengths are larger for the high-res nested LES. This suggests that most of the time the clouds in the high-res nested LES are slightly bigger and more clustered than in the periodic LES.

The second row of Figure 6 shows that the high-res nested LES produces significantly smaller clouds and clear sky areas than the low-res nested LES. This is due to the refinement that occurs when cloud structures transition from the low-res to the high-res nested LES, as can be seen in the top panel of Figure 1 and the animations in Movies S1 and S2. The high-res nested LES tends to break up larger cloud structures into smaller ones, with patches of clear sky between them, reducing both the mean cloud and mean open sky lengths.

In the third row of Figure 6 a similar trend can be seen. The clouds generated by the low-res nested LES are much smaller than the clouds present in HARMONIE. The median mean open sky length is also smaller for the low-res nested LES. Once again, referring to the top panel of Figure 1 and the animation in Movies S1 and S2, this is due to the refinement of the clouds that occurs as they transition from the lower-resolution HARMONIE simulation to the higher-resolution low-res nested LES. Furthermore, some thin cloud structures present in the HARMONIE simulation are not produced by the low-res nested LES. The comparison between the simulated cloud fields in the top panel of Figure 1 and the MODIS cloud field in the bottom panel showed that, for the displayed time, the refinement occurring in the low-res nested LES is not unrealistic.

The differences between the results for the same simulation but across different analysis domains (rows) arise from both the grid resolution used to calculate the metrics and the specific analysis domain considered. As mentioned previously, the cloud metrics are inherently sensitive to data resolution. The lower-resolution representations of the high- and low-res nested LESs, obtained through the coarse-graining process, show as expected larger values for the mean cloud and clear-sky lengths compared to the results calculated at their native resolutions. This resolution dependency highlights the need to bring the data to comparable resolutions to enable a fair comparison. The method used to obtain a lower-resolution representation of a simulation can influence the results

and although the coarse-graining method applied here does not yield a perfect representation, we believe it provides the fairest and most consistent approach.

Figure 7 shows the time evolution of the cloud metrics. The columns correspond to the same analysis domains as the rows in Figure 6. The rows show the mean cloud length, mean open sky length and cloud fraction metrics. For each analysis domain, the higher-resolution simulation is shown in blue and the lower-resolution simulation in orange.

Comparing the periodic LES and high-res nested LES in the first column shows that the high-res nested LES generally has on average a lower cloud fraction. This is primarily due to the high-res nested LES not exhibiting the rapid increases in cloud fraction observed in the periodic LES on 2, 5, and 7–10 February. After a peak in cloudiness, the periodic LES' cloud fraction drops to or below the level of the high-res nested LES. This intermittent cloud cover was also seen and described in Figure 3. The rapid increase/decrease in cloud fraction for the periodic LES results in an increase/decrease in the mean cloud length and a decrease/increase in the mean open sky length. In contrast, the cloud metrics for the high-res nested LES vary much more gradually. When looking at times when the cloud fractions are below 0.5, excluding the cloud fraction peaks during the dates mentioned earlier, the mean cloud and to a lesser extent the mean open sky lengths are larger for the high-res nested LES. This implies that, at these times, the clouds in the high-res nested LES are both larger and more clustered compared to the periodic LES. This is likely due to the clouds being inherited from a larger model, which enables the formation of larger clouds, spaced more heterogeneously throughout the domain. In contrast, the periodic LES is forced horizontally in a homogeneous manner and as suggested by the domain CAPE values Figure 4, this results in the whole domain being driven toward either stable or unstable conditions, which promotes more intermittent and homogeneous cloud formation.

The second column of Figure 7 shows that the cloud fractions in the high- and low-res nested LESs are very similar, with the low-res LES having a slightly higher average cloud fraction. The mean cloud and open sky lengths are larger for the low-res nested LES. The higher mean cloud and open sky lengths while having similar cloud fractions, indicate that the clouds in the low-res nested LES are larger and more clustered compared to the high-res nested LES. This is a consequence of the refinement in cloud structures, seen in Figure 1 and Movies S1 and S2, occurring when clouds transition from the lower-resolution LES to the higher-resolution LES. The high-res nested LES tends to break up the clouds inherited from the low-res nested LES, resulting in smaller structures.

In the third column of Figure 7, it can be seen that the cloud fraction in HARMONIE is significantly larger than that in the low-res nested LES. This is due to the presence of large thin cloud layers in HARMONIE which can be seen in Figure 1 and Movies S1 and S2. The absence of these thin cloud layers in the low-res nested LES leads to a considerably lower cloud fraction. This also contributes to a much lower mean cloud length in the low-res nested LES compared to HARMONIE. The mean cloud length is further reduced by the tendency of the low-res nested LES to break up the cloud structures inherited from HARMONIE into smaller fragments. This also causes the mean open sky length of the low-res nested LES to be lower than that of the HARMONIE simulation. However, when comparing the low-res nested LES output to a MODIS image (Figure 1), it is clear that the refined cloud fields with a lower cloud fraction in the low-res nested LES are not unrealistic.

The results for the cloud fraction time series from the open boundary setup show similar characteristics to the nested simulations and the GOES-16 satellite comparison presented by Schulz and Stevens (2023). Although a direct comparison of magnitudes is not possible, since their study employed a satellite simulator, the results of the open boundary setup are closer to their findings than the results of the periodic LES. Schulz and Stevens (2023) also reported that, in their configuration, the simulated cloud cover decreased with increasing resolution. We find a similar trend when comparing the cloud fraction derived at the models' native resolutions. However, we believe this behavior is at least partly an artifact of the resolution dependence of the metric, as the models cannot represent partially cloudy grid cells. When the outputs from our simulations are coarsened to a common resolution, no reduction in cloud fraction is observed between the LES runs (bottom middle panel in Figure 7).

In summary, refinement occurs as clouds transition from lower to higher-resolution simulations in the open boundary setup, leading to smaller mean cloud and open sky lengths. The large scale distribution of the cloud structures is inherited, which results in more organized cloud patterns in the high-res nested LES compared to the periodic LES when cloud fractions are below 0.5, excluding extreme cloud fraction peaks in the periodic LES. In contrast, the periodic LES does not inherit cloud structures from a larger model, but is instead driven solely by

horizontal mean tendencies. These drive the entire domain toward, stable or unstable conditions, promoting the generation of more intermittent and homogeneous cloud fields, with the simulation transitioning rapidly between completely cloudy and cloud free.

4.3. The Potential Influence of Simulation Settings on the Results

Although the periodic LES and high-res nested LES both represent the same test case and are, apart from their boundary implementation and accompanying method of large-scale forcing, similar in setup, they do differ on several other points that could potentially influence cloud organization (Table 1). These include the microphysical scheme, the prescribed CDNC, domain size, the subfilter-scale (SFS) diffusion approach, and the representation of SST. In this section, we discuss each of these aspects and assess to what extent they can account for the differences seen between the two simulations.

The CDNC can influence precipitation formation, which influences the formation of cold pools, that can in turn impact cloud organization. Alinaghi et al. (2025) studied the role of CDNC in mesoscale adjustments of trade-wind cumulus fields using DALES. Their experiments, with CDNCs ranging from 20 to 1,000 cm^{-3}, showed that the extremes of this range lead to distinct differences. Higher CDNC values delayed the onset of precipitation and produced more widely spaced cold pools that interacted less frequently, resulting in more intermittent behavior and more aggregated cloud fields. The CDNC values used here, 50 cm^{-3} for the periodic LES and 70 cm^{-3} for the high-res nested LES, both fall within the intermediate range explored by Alinaghi et al. (2025). The differences found in that range were small and do not explain the more pronounced differences in cloud organization found in this study.

Similar to CDNC, the choice of microphysical scheme can also influence cloud organization. A comparison between the schemes used in the periodic LES (Khairoutdinov & Kogan, 2000) and in the high-res nested LES (Seifert & Beheng, 2001) was carried out by Stevens and Seifert (2008). Using a combination of LES and simple models, they found that the scheme of Khairoutdinov and Kogan (2000) produces precipitation less efficiently than that of Seifert and Beheng (2001). The increased precipitation in the latter was found to reduce the liquid water path and cloud fraction. This behavior is opposite to what is seen in our simulations. The periodic LES, which shows more intermittent precipitation and cloud cover, produces at peak times higher precipitation rates and larger cloud fractions than the high-res nested LES. These contrasting tendencies suggest that differences in the used microphysics schemes are not a dominant contributor to the observed differences in cloud organization.

The two LES configurations also differ in the way they handle SFS diffusion. The high-res nested LES uses the anisotropic formulation of de Roode et al. (2022), while the periodic LES applies traditional isotropic diffusion. The use of the anisotropic formulation reduces the computational costs of the open boundary setup by increasing the integration time step stability threshold. de Roode et al. (2022) compared both approaches in DALES using a fixed vertical grid spacing of 12.5 m and varying horizontal grid spacings between 12.5 and 800 m, resulting in anisotropy factors $r = \Delta x/\Delta z$ between 1 and 64. They found that for large anisotropy factors, the anisotropic scheme dissipates relatively more variance at smaller scales, shifting spectral energy toward larger scales. The anisotropy factor in our high-res nested LES ranges from 7.8 at the surface to 1.3 near the top of the domain. According to de Roode et al. (2022), significant differences appear only when anisotropy factors exceed 16. We therefore expect the influence of the SFS diffusion choice on the results to be small.

The periodic LES uses a smaller horizontal domain than the high-res nested LES, which in principle could limit the size of the clouds it can support (de Roode et al., 2004). The domain size of the periodic LES (150×150 km^2) is comparable to the one used in the Botany shallow cumulus ensemble of Jansson et al. (2023). Their study showed that DALES can produce a range of mesoscale cloud structures in such a domain, which gives us the confidence that the domain size is large enough to produce these type of cloud structures. Furthermore, Lamaakel et al. (2023) conducted four LESs in the trades with varying domain sizes to study the influence of domain size on the simulation results for precipitating shallow cumulus convection. They found that their two smallest simulations (40×40 km^2 and 80×80 km^2) were too small to adequately capture mesoscale (cloud) structures, which are about 100 km long. However, the flow statistics and length scales converged for the two larger simulations (160×160 km^2 and 330×330 km^2), with little difference between them. These results give us confidence that the 150×150 km^2 periodic domain presented in this research is sufficiently large enough to produce mesoscale features that are not limited by domain size.

Table 3
Computing Time Multiplied by Used Processors Divided by Number of Days Simulated

High-res nested LES	Low-res nested LES	Periodic LES
1,752.7 days	1,361.0 days	1,247.6 days

Finally, the high-res nested LES is driven by spatially heterogeneous SSTs, while the periodic LES uses a spatially homogeneous SST. Chen et al. (2025) showed that warm SST anomalies can locally enhance cloud formation. Whether this has a systematic effect on the domain-mean cloudiness depends on whether the impacts of warm and cold anomalies balance each other. While Chen et al. (2025) focused on warm anomalies only, they expect the opposite behavior for cold anomalies. This is supported by the satellite study of Chen et al. (2023) conducted in the EUREC^{4}A region that suggest that, on average, the net impact of SST anomalies on cloudiness is small. We therefore do not expect the use of spatially heterogeneous SST forcing to be a dominant contributor to the differences observed between the periodic LES and high-res nested LES.

In summary, although the simulations differ in several aspects besides their boundary formulation, previous studies suggest that it is reasonable to assume that the influence of these factors on cloud organization is minor for the setups used in this study. We therefore conclude that the observed differences in cloud organization are dominated by the treatment of the lateral boundary conditions and the associated large-scale forcing.

4.4. Discussion on the Computational Costs

The realistic LES case studies presented in this paper are computationally demanding and only feasible due to the increasing availability of high-performance computing resources. Here we briefly discuss the differences in computational costs between the periodic and open boundary setups. Table 3 shows the total computing time multiplied by the processors used divided by the number of days simulated for each simulation.

The total computing time of the open boundary setup, the high- and low-res nested LESs combined, is 2.5 times that of the periodic setup. The implementation of the open boundary conditions itself does not significantly increase the computational cost per grid cell and time step, as the same dynamical solvers are employed in both the periodic and open boundary configurations (Liqui Lung et al., 2024). The additional expenses of the open boundary setup arise from practical modeling considerations. Open boundary simulations generally require larger domains to allow mesoscale variability to develop and to avoid artificial boundary influences. For these reasons, the configuration used here also includes the intermediate low-res nested LES. Consequently, the total computational cost increases due to (a) the larger high-res nested LES domain compared to the periodic LES domain and (b) the addition of the low-res nested LES.

The domain sizes chosen for both the high- and low-res nested LESs are largely motivated by the requirements of the EUREC^{4}A MIP framework. It is likely that slightly smaller domains could have been used without substantially compromising the results. Nevertheless, the computational costs highlight that periodic simulations continue to have a strong role within the LES community, particularly for research questions where the periodicity constraint does not introduce significant physical limitations. As well as for conducting idealized experiments, where one wants to study processes under easily described and easily varied conditions rather than with fully specified boundary conditions from a specific day or case.

5. Conclusions

This paper presents an open boundary setup, that consists of a high-resolution (high-res) LES that is one-way nested in a low-resolution (low-res) LES. The results of the high-res nested LES are compared to the LES results from Savazzi et al. (2023) that uses periodic lateral boundary conditions. Both setups are driven by the regional weather model HARMONIE-AROME: the periodic LES via domain-averaged tendency profiles, and the open boundary setup via the boundaries of the low-res nested LES. The goal of this paper is to determine the influence of open boundary conditions and a nested setup on the generated cloud fields, and to examine how cloud structures change as they transition to higher-resolution simulations within the open boundary setup.

Comparing the high-res nested LES to the periodic LES, both generate similar domain-averaged background conditions and a daily cycle, which consists of maximum cloud cover around sunrise, followed by precipitation that partly dissolves the clouds, leading to reduced cloud cover around sunset. These findings agree with the radar observational study of Vial et al. (2023). However, the magnitude of this daily cycle is much larger for the periodic LES, with days starting completely cloudy and ending with clear skies. Clouds are more intermittent, penetrate deeper and rainfall is more intense. The rapid growth of clouds in the periodic LES is also accompanied

by an increase in cloud base height. The high-res nested LES, on the other hand, maintains a much more constant cloud cover, with cloud top and base varying more gradually. Vial et al. (2023) reported that the variation in cloud cover is mainly in the deep clouds, whereas the shallow clouds are more constant throughout the day. This behavior is more accurately produced by the open boundary setup as the periodic LES produces an intermittent cloud cover throughout its entire vertical column.

It was found that the strong intermittent cloud cover of the periodic LES is accompanied by strong variations in CAPE, CIN, and vertical velocity variance throughout the majority of the domain. In contrast, cloudy periods in the high-res nested LES are accompanied by more localized variations in CAPE and CIN. This supports our hypothesis that the horizontally-averaged large-scale forcing applied to the periodic LES drives the whole domain toward stable or unstable conditions, promoting the generation of more homogeneous and intermittent cloud fields. The large-scale forcing through the lateral boundaries as used in the open boundary setup on the other hand allows for greater spatial variability and a more realistic evolution of local instability.

The more intermittent behavior of the periodic LES results in a greater spread of observed cloud structures. It rapidly shifts between very cloudy scenes with large clouds and scenes with few, small clouds scattered throughout the domain. In contrast, the cloud characteristics of the high-res nested LES vary less and more gradually. During non-peak cloud fraction periods in the periodic LES, when cloud fractions in both simulations are below 0.5 and more in the range of values reported by Vial et al. (2023), Schulz and Stevens (2023), the clouds in the high-res nested LES tend to be larger, more clustered, and more heterogeneous across the domain, compared to the more homogeneously distributed clouds in the periodic LES.

Within the open boundary setup itself, it was found that refinement occurs as clouds transition from lower to higher-resolution simulations, breaking up the inherited clouds into smaller fragments. The location and distribution of the cloud structures on a larger scale remain conserved. When transitioning from the low- to high-res nested LES, the cloud fraction stays roughly the same, whereas there is a significant drop in cloud fraction when transitioning from HARMONIE-AROME to the low-res nested LES. This drop is explained by the lack of thin cloud layers that are present in HARMONIE-AROME but not produced by the low-res nested LES.

Overall, our findings show that LES with open boundary conditions employed in a repeated nested setup captures a more spatially variable and gradual evolution of cloud fields compared to simulations with periodic lateral boundaries. By allowing the full atmospheric state from a lower-resolution model to enter through the boundaries, the open boundary setup enables more localized interactions between cloud dynamics and large-scale forcing. This results in larger, more organized, and less intermittent cloud structures that are more in line with previous observational studies. While implementing open boundaries and employing a nested setup increases model complexity, our results suggest that for large-domain LES, particularly those designed for comparison with observations, it might result in more accurate results as opposed to periodic LES with large-scale tendencies.

Despite these advantages, several challenges remain when applying open boundary conditions in LES. Defining a suitable domain configuration is nontrivial, as the boundaries must be placed far enough from the area of interest to minimize the influence of spinup and transition zones where turbulence is not yet fully developed. To minimize spinup artifacts, high-frequency boundary data is required to adequately capture the temporal variability of the inflow, which can be demanding both in terms of storage and computational cost. Addressing these aspects is essential for ensuring stable and realistic results. An online coupling framework and an accessible interface to help set up the domains, such as recently implemented in PALM by Kadasch et al. (2021), would help with this.

Appendix A: DALES Coupler

In this appendix, the processes of coupling DALES to HARMONIE (low-res nested LES) and DALES to itself (high-res nested LES) are described. Simulations are coupled through input files. We will address the simulation from which the input files are generated as the "parent" simulation and the simulation that uses the input files as the "child" simulation. The coupling is one-way and offline, which means that information flows only from parent to child and not the other way around. The process follows three main steps. First, the parent simulation is conducted. Second, the input files for the child simulation are created from the parent output. Third, the child simulation is conducted using these input files. The required input files include:

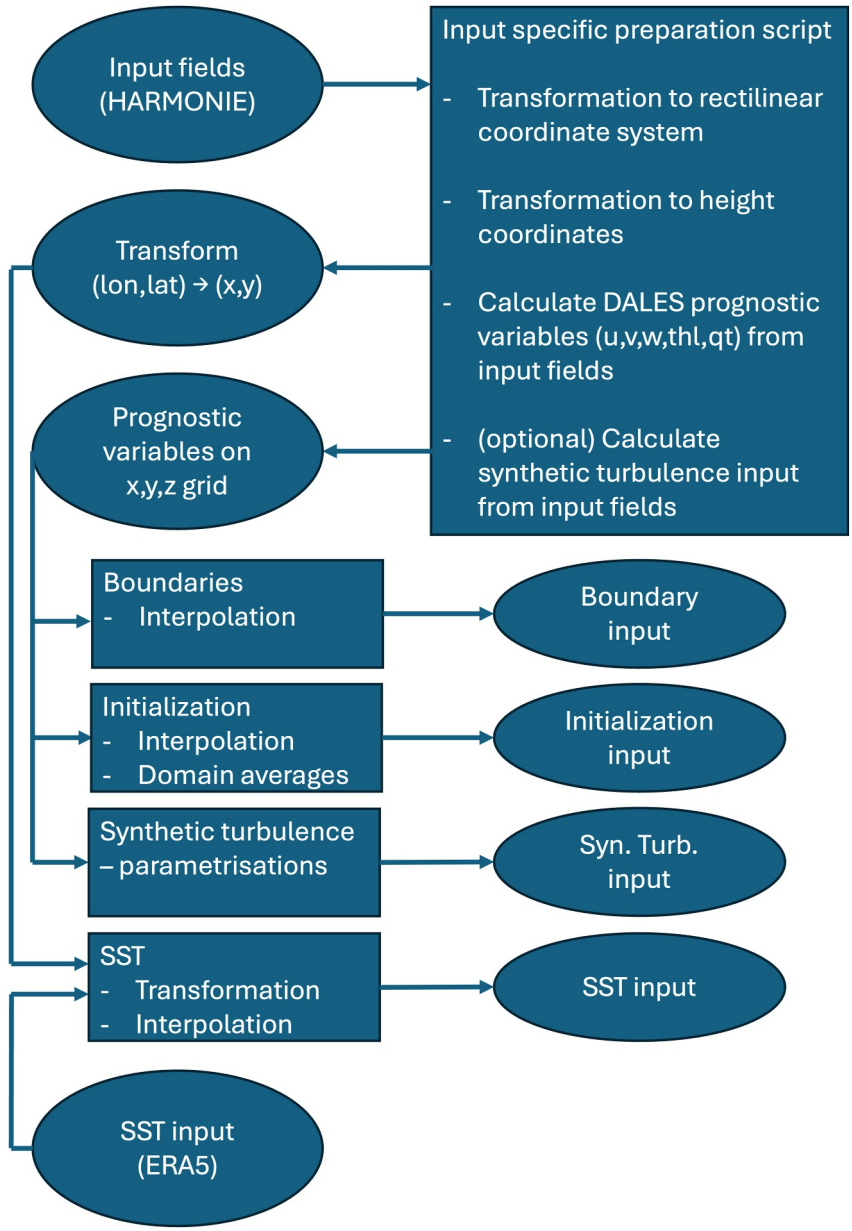

Figure A1. Illustration of the steps taken to couple DALES to HARMONIE using it's open boundary conditions.

1. A file specifying the prognostic fields at the boundaries with optional synthetic turbulence input for the duration of the simulation.
2. A file specifying the initial 3D state of the prognostic variables.
3. A file specifying the sea surface temperatures for the duration of the simulation.
4. A file giving atmospheric profiles above the simulation domain for the radiation scheme.
5. A file with the slab averaged profiles of the initial state.

The process for generating these files is illustrated in Figure A1. The python code used to create the input files is provided by Liqui Lung and Jansson (2025).

When the parent output variables are different from DALES' prognostic variables and/or are in a different coordinate system, the first step is to perform a coordinate transformation to a rectilinear grid and to convert the parent output variables to DALES' prognostic variables. This is the case for the HARMONIE output, which is used as a parent for the low-res nested LES. The HARMONIE output used are temperature (t_a), the three velocity

components (u_a, v_a, w_a), specific humidity (hus), cloud liquid water (clw) and pressure (p). The output is given in a local horizontal rectilinear coordinate system and uses pressure coordinates for the vertical. The output comes with a transform that gives the relation between the local system (x, y) and the WGS84 coordinate system (lon, lat). As a first step, the coordinate transform is translated such that the origin aligns with the South-West corner of the DALES domain. Next, the pressure levels are transformed into height levels and interpolated onto a regular height grid. Finally, temperature, pressure, specific humidity and cloud liquid water are converted to liquid water potential temperature θ_l and total specific water q_t. Total specific water is defined as $q_t = hus + clw$.

To obtain the liquid water potential temperature, the Exner function (Π) is calculated. The Exner functions is obtained by constructing the reference density profile used by DALES from the initial HARMONIE surface pressure and surface liquid water potential temperature fields averaged over the DALES domain. A reference pressure profile is obtained by using the reference density profile together with the initial HARMONIE temperature, specific humidity and cloud liquid water fields horizontally averaged over the DALES domain. The Exner function is obtained with the reference pressure profile. The liquid water potential temperature is then defined as $\theta_l = \frac{t_a}{\Pi} - \frac{L_v}{c_p}\frac{clw}{\Pi}$. By defining the Exner function this way, it remains constant with time and equal to the Exner function used by DALES. This means that converting between temperature and liquid water potential temperature can be easily done using the Exner function and omits changes in pressure.

The boundary input is obtained by interpolating the converted HARMONIE fields to the location of the DALES boundaries. The initial state is obtained by interpolating the converted HARMONIE fields to the DALES grid. The initial profiles are obtained by horizontally averaging the initial state. The atmospheric profiles used for the radiation scheme are obtained by horizontally averaging HARMONIE's humidity and temperature fields over the domain of DALES and temporally avering over a 6−hour period. The sea surface temperatures are taken from ERA5. They are transformed and interpolated to DALES' local rectilinear grid using the translated coordinate transform.

DALES' open boundary conditions have the option to add synthetic turbulence to the boundary fields (Liqui Lung et al., 2024), which requires additional input. For each height level the routine needs the components of the velocity covariance matrix $\left(\overline{u_i' u_j'}\right)$, the variances of the liquid water potential temperature $\left(\overline{\theta_l'^2}\right)$ and total specific humidity $\left(\overline{q_t'^2}\right)$ and the covariances of the liquid water potential temperature and total specific humidity with the vertical velocity ($\overline{\theta_l' w'}$, $\overline{q_t' w'}$). Currently, boundary layer parametrisations are used to obtain these (co)variances from the surface fluxes of heat and momentum and the subgrid TKE output of HARMONIE, horizontally averaged over the DALES domain. The additional input is added in the boundary input file. The velocity variances are assumed to be equal and are defined by Equation A1.

$$\overline{u'^2} = \overline{v'^2} = \overline{w'^2} = \frac{2}{3} tke \tag{A1}$$

The covariance between the horizontal and vertical velocity components are defined by Equations A2 and A3.

$$\overline{u'w'} = \begin{cases} (1 - z/z_i)\, u_*^2 & \text{if } z \le z_i \\ 0 & \text{otherwise} \end{cases} \tag{A2}$$

$$\overline{v'w'} = \begin{cases} (1 - z/z_i)\, v_*^2 & \text{if } z \le z_i \\ 0 & \text{otherwise} \end{cases} \tag{A3}$$

In Equations A2 and A3 u_* and v_* are the horizontal surface friction velocities, z the height coordinate and z_i the inversion layer height. The covariance between the two horizontal velocity components is set to the smallest absolute value for which the covariance matrix $\overline{u_i' u_j'}$ is positive definite. The positive definite criteria assures that the eigenvalues used in the synthetic turbulence routine are real and positive. The covariance between the vertical velocity and the liquid water potential temperature is defined by Equation A4.

$$\overline{\theta_l' w'} = \begin{cases} w'\theta_s' \left(1 - 1.2\frac{z}{z_i}\right) & \text{if } z \leq z_i \\ 0 & \text{otherwise} \end{cases} \tag{A4}$$

In Equation A4 $w'\theta_s'$ is the surface liquid water potential temperature flux. The liquid water potential temperature variance is defined by Equation A5.

$$\overline{\theta_l'^2} = \begin{cases} \frac{z}{70}\left(T_*\left(\frac{z}{z_i}\right)^{-\frac{1}{3}}\right)^2 & \text{if } z \leq 70 \\ \left(T_*\left(\frac{z}{z_i}\right)^{-\frac{1}{3}}\right)^2 & \text{if } 70 < z \leq z_i \\ 0 & \text{otherwise} \end{cases} \tag{A5}$$

In Equation A5 the temperature scale is given by $T_* = \frac{\overline{w'thl'}_s}{w_*}$, with w_* being the convective vertical velocity scale. A damping factor for the first 70 m is added to not add too much variance near the surface. The total specific humidity variance and the covariance between the total specific humidity and the vertical velocity are set to zero, which means that no synthetic turbulence will be added for the total specific humidity.

When the parent model is a different DALES simulation, as is the case for the high-res nested LES, no coordinate transformation or variable conversion is required. 2D cross-section output from the parent model at the location of the boundaries of child model is interpolated and used to obtain the required boundary input files. The initialization input is obtained by interpolating the initialization input of the parent model. The same initialization and radiation profiles are used as the parent model. For the simulations given in this paper, no synthetic turbulence was used for the high-res nested LES, as the parent output interval was much more frequent and already contained turbulent structures.

Conflict of Interest

The authors declare no conflicts of interest relevant to this study.

Availability Statement

The current version of DALES is available from the project website: https://github.com/dalesteam/dales under the GNU General Public License. The exact version of the model used for the nested simulations is archived on Zenodo https://doi.org/10.5281/zenodo.14905895 (Arabas et al., 2024), as is the output from the periodic, open boundary and HARMONIE simulations https://doi.org/10.5281/zenodo.15138400 (Liqui Lung et al., 2025). The scripts used to generate the boundary input can be found here https://doi.org/10.5281/zenodo.15128213 (Liqui Lung & Jansson, 2025).

Acknowledgments
We acknowledge the use of ECMWF's computing and archive facilities, the funding provided by the Australian Research Council Centre of Excellence for Climate Extremes (CE170100023) and the support of the Ruisdael Observatory, a scientific research infrastructure which is (partly) financed by the Dutch Research Council (NWO, Grant 184.034.015). We would also like to thank Alessandro Savazzi for discussing his periodic simulations, Martin Janssens for his insights and assistance with his cloud metrics package, and Bert van Ulft for providing the HARMONIE-AROME simulation used in this research. Lastly, we thank the anonymous reviewers for their constructive and helpful comments, which improved the quality of this manuscript. Open access publishing facilitated by Monash University, as part of the Wiley - Monash University agreement via the Council of Australasian University Librarians.

References

Alinaghi, P., Jansson, F., Blázquez, D. A., & Glassmeier, F. (2025). Cold pools mediate mesoscale adjustments of trade-cumulus fields to changes in cloud droplet number concentration. *Atmospheric Chemistry and Physics*, *25*(12), 6121–6139. https://doi.org/10.5194/acp-25-6121-2025

Arabas, S., Axelsen, S., Attema, J., Azizi, V., Beets, C., Boeing, S. J., et al. (2024). Dalesteam/dales: Dales-eurec4a-mip [Software]. *Zenodo*. https://doi.org/10.5281/zenodo.14905895

Bengtsson, L., Andrae, U., Aspelien, T., Batrak, Y., Calvo, J., de Rooy, W., et al. (2017). The HARMONIE–AROME model configuration in the ALADIN–HIRLAM NWP system. *Monthly Weather Review*, *145*(5), 1919–1935. https://doi.org/10.1175/MWR-D-16-0417.1

Blossey, P. N., Bretherton, C. S., Zhang, M., Cheng, A., Endo, S., Heus, T., et al. (2013). Marine low cloud sensitivity to an idealized climate change: The CGILS LES intercomparison. *Journal of Advances in Modeling Earth Systems*, *5*(2), 234–258. https://doi.org/10.1002/jame.20025

Bony, S., Stevens, B., Ament, F., Bigorre, S., Chazette, P., Crewell, S., et al. (2017). EUREC^{4}A: A field campaign to elucidate the couplings between clouds, convection and circulation. *Space Sciences Series of ISSI*, 357–396. https://doi.org/10.1007/978-3-319-77273-8_16

Borgnino, M., Desbiolles, F., Meroni, A. N., & Pasquero, C. (2025). Lower tropospheric response to local sea surface temperature anomalies: A numerical study in the EUREC^{4}A region. *Geophysical Research Letters*, *52*(1), e2024GL112294. https://doi.org/10.1029/2024GL112294

Chen, X., Dias, J., Wolding, B., Blossey, P. N., DeMott, C., Pincus, R., & Thompson, E. J. (2025). Impacts of weak sea surface temperature warm anomalies on local trade cumulus cloudiness in large eddy simulations. *Journal of Advances in Modeling Earth Systems*, *17*(7), e2024MS004778. https://doi.org/10.1029/2024MS004778

Chen, X., Dias, J., Wolding, B., Pincus, R., DeMott, C., Wick, G., et al. (2023). Ubiquitous sea surface temperature anomalies increase spatial heterogeneity of trade wind cloudiness on daily time scale. *Journal of the Atmospheric Sciences*, *80*(12), 2969–2987. https://doi.org/10.1175/JAS-D-23-0075.1

Deardorff, J. (1972). Numerical investigation of neutral and unstable planetary boundary layers. *Journal of the Atmospheric Sciences*, *29*(1), 91–115. https://doi.org/10.1175/1520-0469(1972)029⟨0091:NIONAU⟩2.0.CO;2

Deardorff, J. W. (1980). Stratocumulus-capped mixed layers derived from a three-dimensional model. *Boundary-Layer Meteorology*, *18*(4), 495–527. https://doi.org/10.1007/BF00119502

Denby, L., & Janssens, M. (2023). Cloudmetrics [Software]. *Zenodo*. https://doi.org/10.5281/zenodo.10154543

de Roode, S. R., Duynkerke, P. G., & Jonker, H. J. J. (2004). Large-eddy simulation: How large is large enough? *Journal of the Atmospheric Sciences*, *61*(4), 403–421. https://doi.org/10.1175/1520-0469(2004)061⟨0403:LSHLIL⟩2.0.CO;2

de Roode, S. R., Siebesma, A. P., Jansson, F., & Janssens, M. (2022). Dependency of mesoscale organization on grid anisotropy in large-eddy simulations of convective boundary layers at gray zone resolutions. *Journal of Advances in Modeling Earth Systems*, *14*(11), e2022MS003095. https://doi.org/10.1029/2022MS003095

de Rooy, W. C., Siebesma, P., Baas, P., Lenderink, G., de Roode, S. R., de Vries, H., et al. (2022). Model development in practice: A comprehensive update to the boundary layer schemes in HARMONIE-AROME cycle 40. *Geoscientific Model Development*, *15*(4), 1513–1543. https://doi.org/10.5194/gmd-15-1513-2022

Forster, P., Storelvmo, T., Armour, K., Collins, W., Dufresne, J.-L., Frame, D., et al. (Eds.), Climate change 2021: The physical science basis. Contribution of working group I to the sixth assessment report of the intergovernmental panel on climate change (pp. 923–1054). Cambridge University Press. https://doi.org/10.1017/9781009157896.009

Heinze, R., Dipankar, A., Henken, C. C., Moseley, C., Sourdeval, O., Trömel, S., et al. (2017). Large-eddy simulations over Germany using icon: A comprehensive evaluation. *The Quarterly Journal of the Royal Meteorological Society*, *143*(702), 69–100. https://doi.org/10.1002/qj.2947

Heus, T., van Heerwaarden, C., Jonker, H., Siebesma, A., Axelsen, S., Dries, K., et al. (2010). Formulation of the Dutch atmospheric large-eddy simulation (DALES) and overview of its applications. *Geoscientific Model Development*, *3*(2), 415–444. https://doi.org/10.5194/gmd-3-415-2010

Janssens, M., Jansson, F., Alinaghi, P., Glassmeier, F., & Siebesma, A. P. (2025). Symmetry in mesoscale circulations explains weak impact of trade cumulus self-organization on the radiation budget in large-eddy simulations. *Geophysical Research Letters*, *52*(3), e2024GL112288. https://doi.org/10.1029/2024GL112288

Janssens, M., Vilà-Guerau de Arellano, J., Scheffer, M., Antonissen, C., Siebesma, A. P., & Glassmeier, F. (2021). Cloud patterns in the trades have four interpretable dimensions. *Geophysical Research Letters*, *48*(5), e2020GL091001. https://doi.org/10.1029/2020GL091001

Jansson, F., Janssens, M., Grönqvist, J. H., Siebesma, A. P., Glassmeier, F., Attema, J., et al. (2023). Cloud botany: Shallow cumulus clouds in an ensemble of idealized large-domain large-eddy simulations of the trades. *Journal of Advances in Modeling Earth Systems*, *15*(11), e2023MS003796. https://doi.org/10.1029/2023MS003796

Kadasch, E., Sühring, M., Gronemeier, T., & Raasch, S. (2021). Mesoscale nesting interface of the palm model system 6.0. *Geoscientific Model Development*, *14*(9), 5435–5465. https://doi.org/10.5194/gmd-14-5435-2021

Khairoutdinov, M., & Kogan, Y. (2000). A new cloud physics parameterization in a large-eddy simulation model of marine stratocumulus. *Monthly Weather Review*, *128*(1), 229–243. https://doi.org/10.1175/1520-0493(2000)128⟨0229:ANCPPI⟩2.0.CO;2

Lac, C., Chaboureau, J.-P., Masson, V., Pinty, J.-P., Tulet, P., Escobar, J., et al. (2018). Overview of the MESO-NH model version 5.4 and its applications. *Geoscientific Model Development*, *11*(5), 1929–1969. https://doi.org/10.5194/gmd-11-1929-2018

Lamaakel, O., Venters, R., Teixeira, J., & Matheou, G. (2023). Computational domain size effects on large-eddy simulations of precipitating shallow cumulus convection. *Atmosphere*, *14*(7), 1186. https://doi.org/10.3390/atmos14071186

Lilly, D. (1966). The presentation of small-scale turbulence in numerical simulation experiments. In *Proceedings of IBM Scientific Computing Symposium on Environmental Science 1967* (pp. 195–210). https://doi.org/10.5065/D62R3PMM

Liqui Lung, F., Jakob, C., Siebesma, A. P., & Jansson, F. (2024). Open boundary conditions for atmospheric large-eddy simulations and their implementation in DALES4.4. *Geoscientific Model Development*, *17*(9), 4053–4076. https://doi.org/10.5194/gmd-17-4053-2024

Liqui Lung, F., & Jansson, F. (2025). Franslql/dales_openbc_setup: Eurec4a [Software]. *Zenodo*. https://doi.org/10.5281/zenodo.15128213

Liqui Lung, F., Savazzi, A., & van Ulft, B. (2025). Supporting data for: The influence of open boundary conditions on cloud organization in atmospheric large eddy simulations [Dataset]. *Zenodo*. https://doi.org/10.5281/zenodo.15138400

Platnick, S., Ackerman, S., King, M., Wind, G., Meyer, K., Menzel, P., et al. (2017). Modis atmosphere l2 cloud product (06_l2). NASA MODIS Adaptive Processing System. https://doi.org/10.5067/MODIS/MYD06_L2.061

Rieck, M., Hohenegger, C., & van Heerwaarden, C. C. (2014). The influence of land surface heterogeneities on cloud size development. *Monthly Weather Review*, *142*(10), 3830–3846. https://doi.org/10.1175/MWR-D-13-00354.1

Sato, Y., Nishizawa, S., Yashiro, H., Miyamoto, Y., Kajikawa, Y., & Tomita, H. (2015). Impacts of cloud microphysics on trade wind cumulus: Which cloud microphysics processes contribute to the diversity in a large eddy simulation? *Progress in Earth and Planetary Science*, *2*(1), 23. https://doi.org/10.1186/s40645-015-0053-6

Savazzi, A., Nuijens, L., Rooy, W., Janssens, M., & Siebesma, A. (2023). Momentum transport in organized shallow cumulus convection. *Journal of the Atmospheric Sciences*, *81*, 279–296. https://doi.org/10.1175/JAS-D-23-0098.1

Schulz, H., & Stevens, B. (2023). Evaluating large-domain, hecto-meter, large-eddy simulations of trade-wind clouds using EUREC^{4}A data. *Journal of Advances in Modeling Earth Systems*, *15*(10), e2023MS003648. https://doi.org/10.1029/2023MS003648

Seifert, A., & Beheng, K. D. (2001). A double-moment parameterization for simulating autoconversion, accretion and selfcollection. *Atmospheric Research*, *59–60*, 265–281. https://doi.org/10.1016/S0169-8095(01)00126-0

Siebesma, A. P., Bretherton, C. S., Brown, A., Chlond, A., Cuxart, J., Duynkerke, P. G., et al. (2003). A large eddy simulation intercomparison study of shallow cumulus convection. *Journal of the Atmospheric Sciences*, *60*(10), 1201–1219. https://doi.org/10.1175/1520-0469(2003)60⟨1201:ALESIS⟩2.0.CO;2

Simon, J. S., Bragg, A. D., & Chaney, N. W. (2024). Heterogeneous land-surface effects on TKE and cloud formation: Statistical insights from LES cases. *Journal of Geophysical Research: Atmospheres*, *129*(12), e2023JD039938. https://doi.org/10.1029/2023JD039938

Skamarock, W. C., Klemp, J. B., Dudhia, J., Gill, D. O., Liu, Z., Berner, J., et al. (2021). *A description of the advanced research WRF model version 4.3 (Technical Report Nos. NCAR/TN-556+STR)*. National Center for Atmospheric Research: Boulder, CO, USA. https://doi.org/10.5065/1dfh-6p97

Smirnov, A., Shi, S., & Celik, I. (2001). Random flow generation technique for large eddy simulations and particle-dynamics modeling. *Journal of Fluids Engineering T ASME*, *123*(2), 359–371. https://doi.org/10.1115/1.1369598

Sommeria, G. (1976). Three-dimensional simulation of turbulent processes in an undisturbed trade wind boundary layer. *Journal of the Atmospheric Sciences*, *33*(2), 216–241. https://doi.org/10.1175/1520-0469(1976)033⟨0216:TDSOTP⟩2.0.CO;2

Stevens, B., Bony, S., Farrell, D., Ament, F., Blyth, A., Fairall, C., et al. (2021). EUREC^{4}A. *Earth System Science Data*, *13*(8), 4067–4119. https://doi.org/10.5194/essd-13-4067-2021

Stevens, B., & Seifert, A. (2008). Understanding macrophysical outcomes of microphysical choices in simulations of shallow cumulus convection. *Journal of the Meteorological Society of Japanese Series II*, *86A*, 143–162. https://doi.org/10.2151/jmsj.86A.143

van Zanten, M. C., Stevens, B., Nuijens, L., Siebesma, A. P., Ackerman, A. S., Burnet, F., & Wyszogrodzki, A. (2011). Controls on precipitation and cloudiness in simulations of trade-wind cumulus as observed during RICO. *Journal of Advances in Modeling Earth Systems*, *3*(2). https://doi.org/10.1029/2011MS000056

Vial, J., Albright, A. L., Vogel, R., Musat, I., & Bony, S. (2023). Cloud transition across the daily cycle illuminates model responses of trade cumuli to warming. *Proceedings of the National Academy of Sciences*, *120*(8), e2209805120. https://doi.org/10.1073/pnas.2209805120

Wicker, L. J., & Skamarock, W. C. (2002). Time-splitting methods for elastic models using forward time schemes. *Monthly Weather Review*, *130*(8), 2088–2097. https://doi.org/10.1175/1520-0493(2002)130⟨2088:TSMFEM⟩2.0.CO;2

Zhang, Y., Stevens, B., & Ghil, M. (2005). On the diurnal cycle and susceptibility to aerosol concentration in a stratocumulus-topped mixed layer. *Quarterly Journal of the Royal Meteorological Society*, *131*(608), 1567–1583. https://doi.org/10.1256/qj.04.103